



# Fully catalytic upgrading synthesis of 5-Ethoxymethylfurfural from biomass-derived 5-Hydroxymethylfurfural over recyclable layered-niobium-molybdate solid acid



Fu Yang<sup>a,\*</sup>, Jingjing Tang<sup>a</sup>, Rui Ou<sup>a</sup>, Zengjing Guo<sup>b</sup>, Shuying Gao<sup>c</sup>, Yinzhu Wang<sup>a</sup>, Xuyu Wang<sup>a</sup>, Lei Chen<sup>a</sup>, Aihua Yuan<sup>a,\*</sup>

<sup>a</sup> School of Environmental and Chemical Engineering, Jiangsu University of Science and Technology, Zhenjiang 212003, Jiangsu, China

<sup>b</sup> School of Chemistry and Chemical Engineering, Liaocheng University, Liaocheng, 252000, Shandong, China

<sup>c</sup> State Key Laboratory of Materials-Oriented Chemical Engineering, College of Chemical Engineering, Nanjing Tech University, Nanjing, Jiangsu 210009, China

## ARTICLE INFO

### Keywords:

Polyoxometalates  
Multiple-layer  
Biomass  
Etherification  
Solid acid  
Ethoxymethylfurfural

## ABSTRACT

Biomass-derived resources exploited in depth toward the synthesis of high value-added chemicals is very promising, but still limited by the applicable catalyst. In this paper, we report regulated robust multilayer-like polyoxometalates(Niobium molybdate) specific to the catalytic synthesis of promising 5-Ethoxymethylfurfural (EMF). The present solid acid catalysts resulted from precisely-tuned compositions of Nb and Mo toward acquiring controlled Brønsted acid amounts and interlayer space coupling with specific Lewis acid sites are demonstrated to be the determining factors for tuning conversion and selectivity in the synthesis of EMF, respectively. The characterization results indicate that the increment in Nb moiety is beneficial to produce more accessible acid sites and the enlarged interlayer space in the catalyst, thereby promoting the acid-catalyzed conversion. As a result, the full conversion(Conv. 100%) of 5-hydroxymethylfurfural into the 5-Ethoxymethylfurfural (Select. > 99%) by etherification with ethanol within only 60 min was realized as the record-high yield under the solvent-free condition, far outperforming several traditional catalysts. In addition, the rational 67% yield of EMF was received when using fructose as an initial reactant. Ulteriorly, the resultant catalyst inherits the superior catalytic activity in the substrate expansion experiments in the presence of different alcohols. More importantly, the resulted catalyst shows durable catalytic activity without any activity-loss during the eight recycling, which reveals the huge potential industrial application prospect.

## 1. Introduction

The carbon-containing biomass and its potential derivatives are the unique renewable resource which is capable of serving as both liquid fuels and bulk chemicals [1–10], to remit the crisis of fossil energy depletion. Especially, the promising furan derivate that 5-Ethoxymethylfurfural (EMF) considered being an excellent additive for diesel is capable of being synthesized using acid-assisted catalytic process [11–14] from biomass-derived platforms such as 5-hydroxymethylfurfural (HMF) and fructose. Yet, previous chemical synthesis still failed to receive an ideal yield of EMF owing to the competition of acetalization, polymerization and furan ring opening reactions. The high selectivity of HMF etherification enabled by the catalytic process still relies on the development of highly-efficient catalyst.

Even if the high efficiency of homogeneous molecular acid catalysts

for various chemicals have been demonstrated especially in the utilization and transformation of biomass resources [15,16], their inherent drawbacks to using molecular acid as catalysts, such as the cost of separating the acid from the reaction solution and the generation of massive toxic waste, still limit its further practical industrial application at a large-scale. In turn, solid acid catalysts affording massive accessible acid sites have emerged as popular counterpart cater for the appeal of environment demand, thanks to its reusable and readily separable character from the reaction system [17–20]. This developed promising route that using solid acid catalyst offers the opportunity to reduce the impact on the environment and increase profits. In this case, many familiar solid acids such as clay minerals [12], zeolites [21,22], Cs-heteropoly acids [23], sulfated zirconia [24], ion-exchange resins [25], and sulfonated-carbon materials [26] have been investigated to some extent. Even if the catalytic etherification conversion of HMF easily

\* Corresponding author.

E-mail addresses: [fuyang@just.edu.cn](mailto:fuyang@just.edu.cn) (F. Yang), [aihua.yuan@just.edu.cn](mailto:aihua.yuan@just.edu.cn) (A. Yuan).

takes place using acid catalyst, but the yield of EMF still fail to be reached ~100%, thereby remains unsatisfied and challenged for the actual production [22,27–31], which is mainly attributed to the fact that the etherification of HMF leads to the formation of three by-products: levulinic acid (LA), ethyl-4-oxopentanoate (EOP) [23]. For instance, Liu et al. [32] reported heterogeneous Silica-SO<sub>3</sub>H employed for the catalytic etherification of HMF at 100 °C for 10 h, and 96.5% of conversion was observed, but low EMF yield(83.8%) seems not to be satisfied. As such, when using fructose as a reactant, the yield of HMF was 11.2%, and the yield of EMF was only 63.1%. Saravanamurugan et al. [33] used two routes to prepare SO<sub>3</sub>H-SBA-15 catalysts, in which SO<sub>3</sub>H-SBA-15-D was employed at 140 °C for 24 h to obtain HMF conversion of 99% and EMF yield of 3.5%. While the ethyl 4-oxopentanoate (EOP) yield reached 76%. It can be seen that too high temperature or too long reaction time would cause the generated EMF to degrade to EOP. Balakrishnan et al. [34] used p-TSA and 5 mol% H<sub>2</sub>SO<sub>4</sub> as catalysts respectively. After 24 h reacting at 75 °C, the yields of EMF and EOP were 81% and 15%, respectively. Taken together, highly-efficient generation of promising EMF especially for obtaining potential industrial yield standard remains challenged and to be ulteriorly improved. So far, using layered material is one of the fascinating approaches to developing a solid acid catalyst particularly affording accessible Brønsted acid sites with the enhanced activity and selectivity due to the good contact and space confinement-effect between interlayer acid sites and the reactants, where the interlayer space could be acted as mass-transferring region and thus specific to optimizing products distribution through regulating the selectivity of products, which may be promising for the catalytic conversion of biomass-derived platform chemicals, but remains to be studied in depth.

Herein, we reported highly-efficient and recyclable solid acid catalyst that multilayer polyoxometalates(Niobium molybdate catalyst) with the precisely-controlled Nb/Mo compositions to integrate the tuned acid amount and rational interlayer space aiming to efficiently convert and upgrade 5-hydroxymethylfurfural (HMF) to 5-Ethoxymethylfurfural (EMF). The synthetic procedure of developed catalyst was illustrated and displayed in **Scheme 1**. As desired, the prepared niobium molybdate catalyst affords 100% conversion of HMF and > 99% selectivity towards EMF within 60 min when using HMF as the initial reactant, which exhibits tremendous potential industrial application prospect. The catalytic influence factors including catalyst dosage, reaction temperature, and reaction course were meticulously examined to identify the optimal reaction conditions in the presence of the best catalyst. Furthermore, exploring the synthesis of EMF from fructose was further carried out using the aforementioned optimal catalyst under controlled reaction conditions. Finally, the substrate scope expansion experiment based on the optimal catalyst was studied using various alcohols to identify the adaptability of multilayer niobium molybdate for the etherification.

## 2. Experimental section

### 2.1. Chemicals

Lithium carbonate (Li<sub>2</sub>CO<sub>3</sub>, AR), niobium pentoxide (Nb<sub>2</sub>O<sub>5</sub>, AR), molybdenum trioxide (MoO<sub>3</sub>, AR), tungsten trioxide (WO<sub>3</sub>, AR), and tantalum pentoxide (Ta<sub>2</sub>O<sub>5</sub>, AR) were purchased from the Aladdin. 5-hydroxymethylfurfural (HMF) was purchased from Wuhan Lullaby Pharmaceutical Chemical Co., Ltd. 5-Ethoxymethylfurfural (EMF) was purchased from Sigma-Aldrich. Methanol, ethanol, propyl alcohol, isopropanol (99%), *tert*-butanol (99%), isoamyl alcohol (98%), benzyl alcohol and *cyclohexylmethanol* were purchased from Energy Chemical Co., Ltd. All the reagents were used as received without any further purification.

### 2.2. Synthesis and regulation of multilayer-like polyoxometallate HNbMoO<sub>6</sub>

Multilayer-like polyoxometallate LiNbMoO<sub>6</sub> was obtained according to the reported method [35] by the calcination of a stoichiometric mixture of Li<sub>2</sub>CO<sub>3</sub>, Nb<sub>2</sub>O<sub>5</sub>, and MoO<sub>3</sub> at 580 °C for 24 h with one intermediate intensive grinding. The ensuing proton-exchange reaction was carried out by shaking and stirring the resultant LiNbMoO<sub>6</sub> in 1 M HNO<sub>3</sub> at room temperature for 1 week to realize the completed acidification of LiNbMoO<sub>6</sub>.

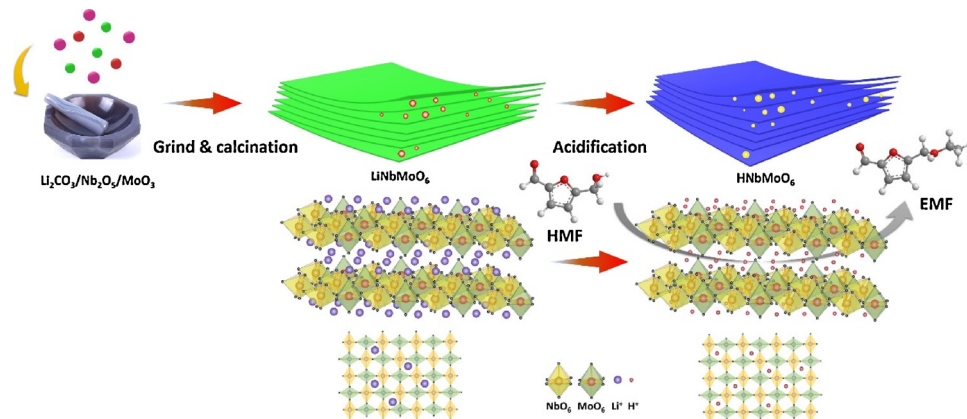
The varied components proportion of Nb and Mo in LiNbMoO<sub>6</sub> were prepared according to the above description but with the controlled stoichiometric mixture of Li<sub>2</sub>CO<sub>3</sub>, Nb<sub>2</sub>O<sub>5</sub>, and MoO<sub>3</sub>(Li: Nb: Mo = 0.7: 0.7: 1.3, 0.85: 0.85: 1.15, 1.15: 1.15: 0.85, 1.3: 1.3: 0.7, molar ratio). The resulted acidifying samples were labeled as H<sub>0.7</sub>Nb<sub>0.7</sub>Mo<sub>1.3</sub>O<sub>6</sub>, H<sub>0.85</sub>Nb<sub>0.85</sub>Mo<sub>1.15</sub>O<sub>6</sub>, H<sub>1.15</sub>Nb<sub>1.15</sub>Mo<sub>0.85</sub>O<sub>6</sub>, and H<sub>1.3</sub>Nb<sub>1.3</sub>Mo<sub>0.7</sub>O<sub>6</sub>. These involved samples were collected for further characterization and ensuing catalytic assessment.

Several comparative catalysts were further prepared by the above similar synthesis method, for example, Li<sub>2</sub>CO<sub>3</sub>(1.8 g), Ta<sub>2</sub>O<sub>5</sub>(11.0 g), MO<sub>3</sub>(7.2 g) were mixed and grinded thoroughly, and then calcined for 24 h at 600 °C. The resulted LiTaMoO<sub>6</sub> was dispersed in certain HNO<sub>3</sub>(1 mol/L) and stirred for a week to realize the completed acidification. Finally, the used catalyst was washed and dried for the following catalytic experiments.

### 2.3. Materials characterizations

The XRD data of the samples were collected using Smartlab TM 9 KW (Rigaku Corporation, Tokyo, Japan) equipped with a rotating anode and Cu K $\alpha$  radiation ( $\lambda = 1.54178 \text{ \AA}$ ).

Temperature-programmed desorption of NH<sub>3</sub> was performed on ChemBET Pulsar TPR/TPD (Quantachrome). 0.05 g of dried sample was



**Scheme 1.** Synthetic description for multilayer polyoxometalate niobium molybdate solid acid catalyst.

pretreated at 300 °C for 1 h by flowing helium gas (99.9%, 30 mL/min). After that, the resulted sample was saturated with anhydrous ammonia (10% NH<sub>3</sub>-90% He mixture gas) at 100 °C for 1 h and was flushed with He gas at the same temperature to remove physisorbed ammonia. Then, the temperature programming desorption was conducted from 100 to 800 °C with a temperature increment of 10 °C/min. The amount of NH<sub>3</sub> evolved was calculated using the calibrated thermal conductivity detector based on the TCD signals.

High-resolution transmission electron microscopy (HRTEM) was operated using a JEM-2010 EX microscope (JEOL, Tokyo, Japan) at an accelerating voltage of 200 kV, equipped with Energy Dispersive X-ray Detector & elemental mapping analysis.

Field emission scanning electron microscopy (FE-SEM) was performed on a Hitachi S4800 Field Emission Scanning Electron Microscopy (Hitachi, Tokyo, Japan). The elemental distribution of materials was determined using energy dispersive X-ray spectroscopy (EDX).

Attenuated total reflectance infrared (ATR-IR) spectroscopy analysis was performed on a Thermo Scientific Nicolet iS50 FT-IR spectrometer integrated with a diamond ATR accessory, and the IR spectra were collected ranging from 4000 to 525 cm<sup>-1</sup>.

Pyridine-IR spectrum was collected by means of a TENSOR 27 apparatus (Bruker, Germany). The sample was pressed into thin wafers and measured in a Pyrex glass cell equipped with CaF<sub>2</sub> windows, and pretreated firstly at 300 °C for 1 h under vacuum (10<sup>-6</sup> Torr) and then cooled to room temperature. Afterwards, the pyridine was flowed through the sample for 30 min and the pyridine adsorption spectrum was recorded after desorption of pyridine at 150 °C.

The X-ray photoelectron spectra (XPS) were recorded on a PHI 5000 Versa Probe X-ray photoelectron spectrometer (ULVAC-PHI, Kanagawa, Japan) equipped with Al K<sub>α</sub> radiation (1486.6 eV). The reference C1s peak at 284.6 eV was used as the standard.

The niobium and molybdenum contents were examined by a PE Optima 2000DV (PerkinElmer, Waltham, MA, USA) Inductively Coupling Plasma emission spectrometer (ICP).

**Computational Details:** All calculation results were based on the Gaussian 09 package. The density of atom charge(Mulliken) was calculated with the Becke's three-parameter hybrid exchange functional and the Lee-Yang-Parr correlation functional (B3LYP).

### 2.3.1. The acid density of the catalyst

The acid density of catalyst was determined using the potentiometric titration on Metrohm 877 Titrino plus instrument. Typically, the catalyst sample (1000 mg) was added into an acetonitrile solution (60 mL), which was dispersed uniformly in an ultrasonic bath at room temperature for 20 min. After 3 h stirring, the solution was potentiometrically titrated by acetonitrile solution of n-butylamine (0.01 mol/L) using phenolphthalein as an indicative. The received acidic amount of the samples can be quantificationally evaluated by this technique.

### 2.4. Catalytic performance assessment

#### 2.4.1. Upgrading synthesis of EMF from HMF

This reaction was conducted in a pressure bottle, typically, HMF (0.126 g, 1.0 mmol), ethanol(5 ml), and certain catalyst were added into 35 ml of pressure bottle. Subsequently, the reactor was heated to a certain temperature and reacted for a desirable time. Finally, the resulted mixture was filtered and diluted with the ethanol for the HPLC analysis. High-Performance Liquid Chromatogram (HPLC, Agilent 1200) is equipped with an organic acid column (Bio-Rad Aminex HPX-87 H) and an ultraviolet detector. The calculated catalytic results are based on the external standard method using the external standard curves(Fig. S1, S3).

$$\text{HMF conversion (\%)} = \frac{\text{moles of HMF}}{\text{moles of starting HMF}} \times 100\% \quad (1)$$

$$\text{EMF Selectivity (\%)} = \frac{\text{moles of EMF}}{\text{moles of starting HMF}} \times 100\% \quad (2)$$

$$\text{EMF Yield (\%)} = \text{HMF conversion} \times \text{EMF Selectivity} \times 100\% \quad (3)$$

#### 2.4.2. Upgrading synthesis of EMF from fructose

This catalytic upgrading synthesis of EMF from the fructose was further evaluated in a pressure bottle. Typically, fructose(1.0 mmol), ethanol(5 ml), and a certain amount of catalyst were added into 35 ml of pressure bottle. Subsequently, the batch reactor was heated to a certain temperature and reacted for desirable reaction time. Finally, the resulted mixture was filtered and diluted with the ethanol for the HPLC analysis. High-Performance Liquid Chromatogram (HPLC, Agilent 1200) is equipped with an organic acid column (Bio-Rad Aminex HPX-87 H) and an ultraviolet detector. The calculated catalytic results are based on the external standard method using the external standard curves (Fig. S2, S3)

$$\text{Fructose conversion (\%)} = \frac{\text{moles of Fructose}}{\text{moles of starting fructose}} \times 100\% \quad (4)$$

$$\text{EMF selectivity (\%)} = \frac{\text{moles of EMF}}{\text{moles of starting fructose}} \times 100\% \quad (5)$$

$$\text{EMF Yield (\%)} = \text{Fructose conversion} \times \text{EMF Selectivity} \times 100\% \quad (6)$$

#### 2.4.3. The NMR analysis of EMF

5-Ethoxymethylfurfural (EMF), a yellow oil-like liquid, is derived from the catalytic conversion with HMF and ethanol, NMR analysis results is displayed as follows : <sup>1</sup>H NMR (400 MHz, DMSO-d6) δ 9.58 (s, 1 H), 7.51 (d, J = 3.5 Hz, 1 H), 6.72 (d, J = 3.5 Hz, 1 H), 4.51 (s, 1 H), 3.51 (q, J = 7.0 Hz, 1 H), 1.14 (t, J = 7.0 Hz, 1 H). <sup>13</sup>C NMR (100 MHz, DMSO-d6) δ/ppm 178.07, 158.31, 152.16, 123.70, 111.47, 65.41, 63.68, 14.78.

### 2.5. Recycling of catalyst

The recycling and reusing experiment was conducted after the complete reaction, and the catalyst was recovered by centrifugation. The recovered catalyst was washed three times with ethanol and deionized water and followed by drying at 80 °C overnight in a vacuum oven. The recovered catalyst was reused for the next cycle with the same procedure.

## 3. Results and discussion

The crystal structure of polyoxometalate was examined to determine the successful synthesis of HNbMoO<sub>6</sub> based on the wide-angle XRD results. As shown in Fig. 1a, the XRD patterns present several typical well-defined diffraction peaks centered at 26.74°, 30.20°, 35.79°, and 38.19°, which is in good agreement with reported HNbMoO<sub>6</sub>, [35] indicating the successful synthesis of typical HNbMoO<sub>6</sub>. Notably, even with the elemental-tuning proportion between Nb and Mo from 0.7/1.3 to 1.3/0.7, these major diffraction peaks still existed and reserved as the main controlled crystals, verifying the dominant crystal unit structure of initial HNbMoO<sub>6</sub>. However, some impurity weak diffraction peaks emerged in the case of H<sub>1.3</sub>Nb<sub>1.3</sub>Mo<sub>0.7</sub>O<sub>6</sub> and H<sub>0.7</sub>Nb<sub>0.7</sub>Mo<sub>1.3</sub>O<sub>6</sub>, indicating the presence of heterogeneous phase crystal structure including Nb<sub>2</sub>O<sub>5</sub> or Mo<sub>2</sub>O<sub>3</sub> [36], and damage of pristine crystal unit in the HNbMoO<sub>6</sub> with the excessive introduction of Nb or Mo in the entire catalyst sample, thereby perturbing the initial crystal structure. On the other hand, since d-spacing is regarded as an important characteristic for the layered compounds, the d values of all acidifying samples were calculated based on the Bragg equation  $\lambda = 2dsin\theta$ . The (001) peak positions of H<sub>1-x</sub>Nb<sub>1-x</sub>Mo<sub>1+x</sub>O<sub>6</sub> samples in the XRD curves were observed for the tiny shift to lower angles with increasing niobium

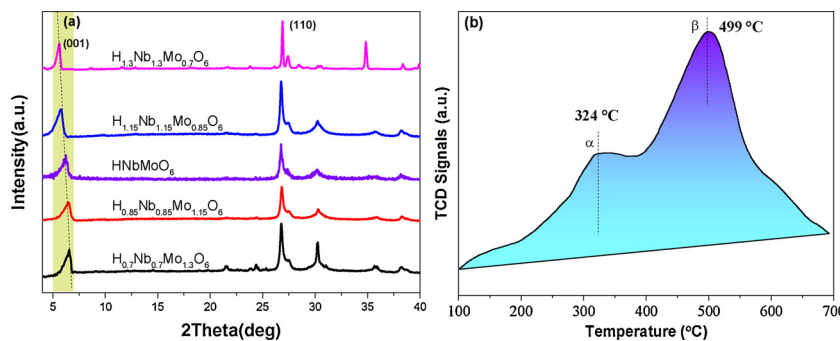


**Fig. 1.** Wide-angle XRD patterns (a) of the involved comparative samples  $H_{1-x}Nb_{1-x}Mo_{1+x}O_6$  and NH<sub>3</sub>-TPD Profile(b) of HNbMoO<sub>6</sub>.

**Table 1**

Basal Spacing of  $H_{1-x}Nb_{1-x}Mo_{1+x}O_6$  obtained from XRD Patterns.

Catalysts	$2\theta_{(001)}$	basal spacing (Å)	interlayer space (Å)
$H_{0.7}Nb_{0.7}Mo_{1.3}O_6$	6.60	13.4	6.3
$H_{0.85}Nb_{0.85}Mo_{1.15}O_6$	6.48	13.6	6.5
HNbMoO <sub>6</sub>	6.28	14.1	7.0
$H_{1.15}Nb_{1.15}Mo_{0.85}O_6$	5.82	15.2	8.1
$H_{1.3}Nb_{1.3}Mo_{0.7}O_6$	5.63	15.7	8.6

content, indicating the gradual increment of the interlayer space with more niobium content. Accordingly, the basal spacing of the samples derived from the above-calculated results is summarized in Table 1. Because the thickness of the Nb-Mo oxide sheets was 7.1 Å (assume the thickness of the laminate is constant in different Nb/Mo proportion) [36], This present expansion of the interlayer spacing ranging from 6.3 to 8.6 Å with increased niobium content probably resulted from an increase in the proton density of the interlayer and hydration degree of interlayer protons, which thereby compensated for the negative charge of the Nb-Mo oxide sheets. This result further indicates the tuning of Nb/Mo proportion largely affect the microstructure of catalyst, which probably generates the regulation effect of molecule diffusion, based on the molecular size adaptability in the reaction space.

The acid property of pristine HNbMoO<sub>6</sub> was inspected as the typical example based on the NH<sub>3</sub> temperature-programmed desorption results, the prepared hydrazine molybdate has two types of acidic sites, and the two NH<sub>3</sub> desorption peaks correspond to the positions at 324 °C and 499 °C, respectively, which attributes the medium acid center and a strong acid center existed in the outer-layer and interlayer of layered structures. This is in contrast to some of the reported acid catalysts (e.g. 360 °C for H-ZSM5) [37] in acid strength, where the acid sites present are moderately strong. And compared to the two acid sites at 324 °C and 499 °C, the relatively stronger acid sites at 499 °C accounted for a higher proportion in the total catalyst, which seems more helpful to get good catalytic activity in the etherification of HMF. Thereinto, the weak acidic sites should be originated from the external surface, while the strong acidic sites correspond to that in the bulk space. This is because the acid strength of the exfoliated nanosheets was lower than that of bulk powders according to the reported literature [38]. Additionally, the absolute presence of Brønsted acid site on the acidified sample can be observed and verified based on the measured Pyridine-IR spectrum of  $H_{1.15}Nb_{1.15}Mo_{0.85}O_6$  (Fig. 4S), specifically, the pyridine absorption peak at 1537 cm<sup>-1</sup> clearly correspond to the Brønsted acid site [39], which is the direct evidence for the successful synthesis of solid niobium molybdate possessing rich protonic acid. Besides, Lewis acid site corresponding to absorption peak at 1445 cm<sup>-1</sup> was also clearly observed, which should ascribe to existence of metal moiety Nb and Mo and their d empty orbital.

To reflect the variation of interlayer moieties in the acidification process with H proton, the IR spectra of niobium molybdate samples were collected and presented in Fig. 2. With regarding layered niobium-

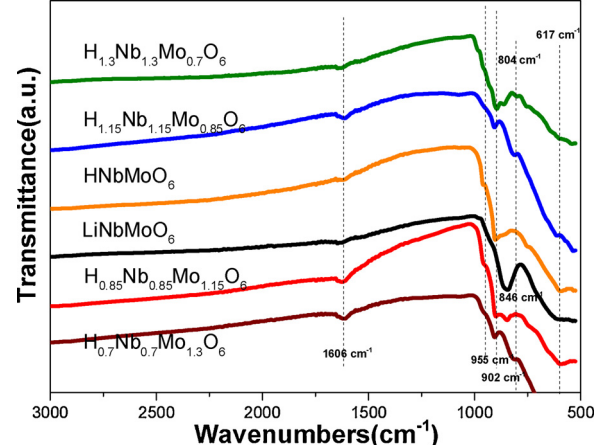


**Fig. 2.** IR spectra of series of polyoxometalate niobium molybdate composites.

based composite oxides, although Nb element exists in the form of NbO<sub>6</sub> unit, the vibration absorption of terminal Nb = O bond is significantly influenced by adjacent cationic elements [40], taking LiNbMoO<sub>6</sub> as the example, the Nb = O band was located at ca. 850 cm<sup>-1</sup>. When the cations of the interlayer (Li<sup>+</sup>) in LiNbMoO<sub>6</sub> were exchanged by H<sup>+</sup> ions, the Nb = O bands shifted and split to 902, and 804 cm<sup>-1</sup>, respectively. In addition, it could be inferred that the hydration degree of the proton has some influence on the Nb = O bands. This result may be induced by the two types of hydrogen ions (H<sup>+</sup> and H<sub>3</sub>O<sup>+</sup>) existing in the interlayer [41], which indicated that the state and distribution of H<sup>+</sup> ions were rather uniform.

The morphology and microstructure of the  $H_{1.15}Nb_{1.15}Mo_{0.85}O_6$  were examined using TEM techniques, as shown in Fig. 3, the multiple-layer cumulated configuration can be observed clearly, which is in good agreement with the reported literature [40]. The  $d_{001}$  lattice fringe corresponding to the real interlayer space of niobium molybdate composites was calculated based on the HRTEM image and is as large as 0.8102 nm, which agrees with the aforementioned XRD results. In addition, the elemental composition was ulteriorly identified via the image information extracted from elemental mapping results, revealing the uniform elemental distribution and definite composition through the thermal sintered process and acidification treatment. To further know the morphology characteristic and elemental composition of pristine HNbMoO<sub>6</sub>, typical SEM and corresponding EDS-mapping technique was utilized for checking the sample (Fig. 4), and sheet-like characteristic at micrometer level and uniform elemental distribution confirmed the success of thermal-sinter process for incorporating the Nb<sub>2</sub>O<sub>5</sub> and Mo<sub>2</sub>O<sub>3</sub> into the multilayer polyoxometalates.

The interaction and existence of H proton in the interlayer of niobium molybdate is the key for the entire catalytic process, accordingly, the high-resolution XPS spectra were utilized to detect the precise elemental information through discerning the valence states of

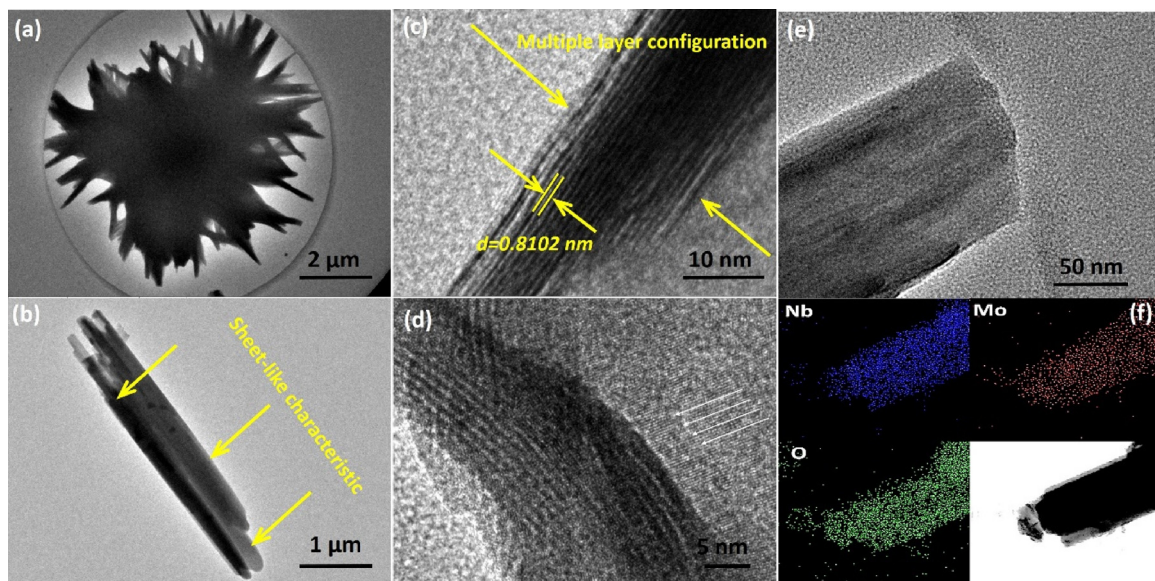


**Fig. 3.** Typical TEM images (a–e) and its elemental mapping results (f) of the resultant  $\text{H}_{1.15}\text{Nb}_{1.15}\text{Mo}_{0.85}\text{O}_6$ .

transition metals in different compounds. First, the elemental composition of this involved sample can be identified to confirm the collective presence of Nb and Mo based on the present survey spectra and disappearance of Li after the protonated process (Fig. 5d). Fig. 5a, b shows the Mo3d and Nb3d doublet spectra of protonated bulk powders. The well-resolved spectral lines at 233.04 and 236.15 eV, typical envelopes of Mo oxides, could be assigned to Mo 3d<sub>5/2</sub> and 3d<sub>3/2</sub> spin-orbit coupling, respectively. As shown in Fig. 5b, the shape, and position of doublet spectrum of  $\text{H}_{1.15}\text{Nb}_{1.15}\text{Mo}_{0.85}\text{O}_6$  powders resembled that of  $\text{MoO}_3$  powders, indicating that the Mo electronic structure in layered tri-rutile-like  $\text{H}_{1.15}\text{Nb}_{1.15}\text{Mo}_{0.85}\text{O}_6$  was identical to that in the orthorhombic layered  $\text{MoO}_3$  compound. Notably, the electronic state of Mo hardly changed before and after the protonated process, while the binding energy of Nb shows the shift towards higher value after the protonated process. This might be associated with the direct interaction of H proton with the Nb atoms rather than the Mo moiety. Therefore, the efficient increment of Nb species in the crystal structure of

$\text{HNbMoO}_6$  should be beneficial to the enhancement of acid amount ( $\text{H}^+$ ). In junction with the previous FT-IR results, the existed formation of H proton as the hydronium protons  $\text{H}_3\text{O}^+$  in the interlayer confined space of molybdate catalyst can be indicated. With the increment of Nb moiety in the materials, the enriched hydronium protons  $\text{H}_3\text{O}^+$  are directly beneficial to expand the interlayer space of niobium molybdate. Therefore, the increased Nb moiety induces the adjusting effect of interlayer space.

### 3.1. Catalytic analysis

To screen the optimal catalyst system, several catalysts such as  $\text{LiNbWO}_6$ ,  $\text{LiTaMoO}_6$ ,  $\text{LiNbMoO}_6$ ,  $\text{HNbWO}_6$ ,  $\text{HTaMoO}_6$ , and  $\text{HNbMoO}_6$  were employed for the catalytic etherification of HMF under the identical reaction conditions, and their catalytic results are shown in Table 2. Compared to the polyoxometalates composites acid, their corresponding lithium salt exhibit the obviously inferior catalytic

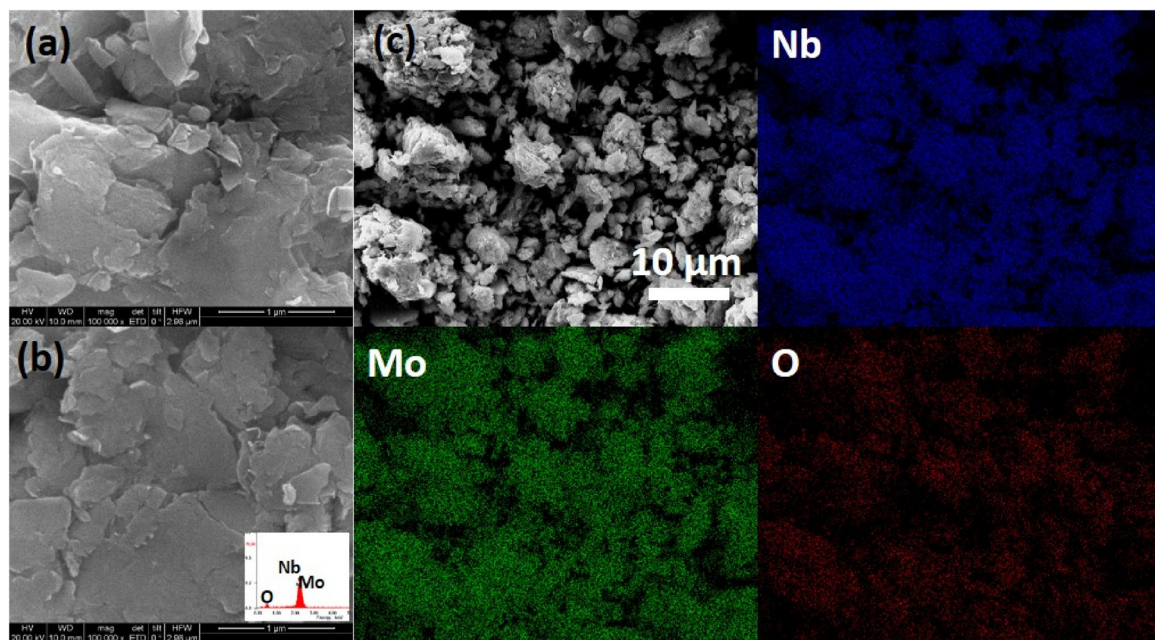


**Fig. 4.** Representative SEM images(EDX, insert) (a) (b) and their corresponding elemental mapping images of  $\text{HNbMoO}_6$ .

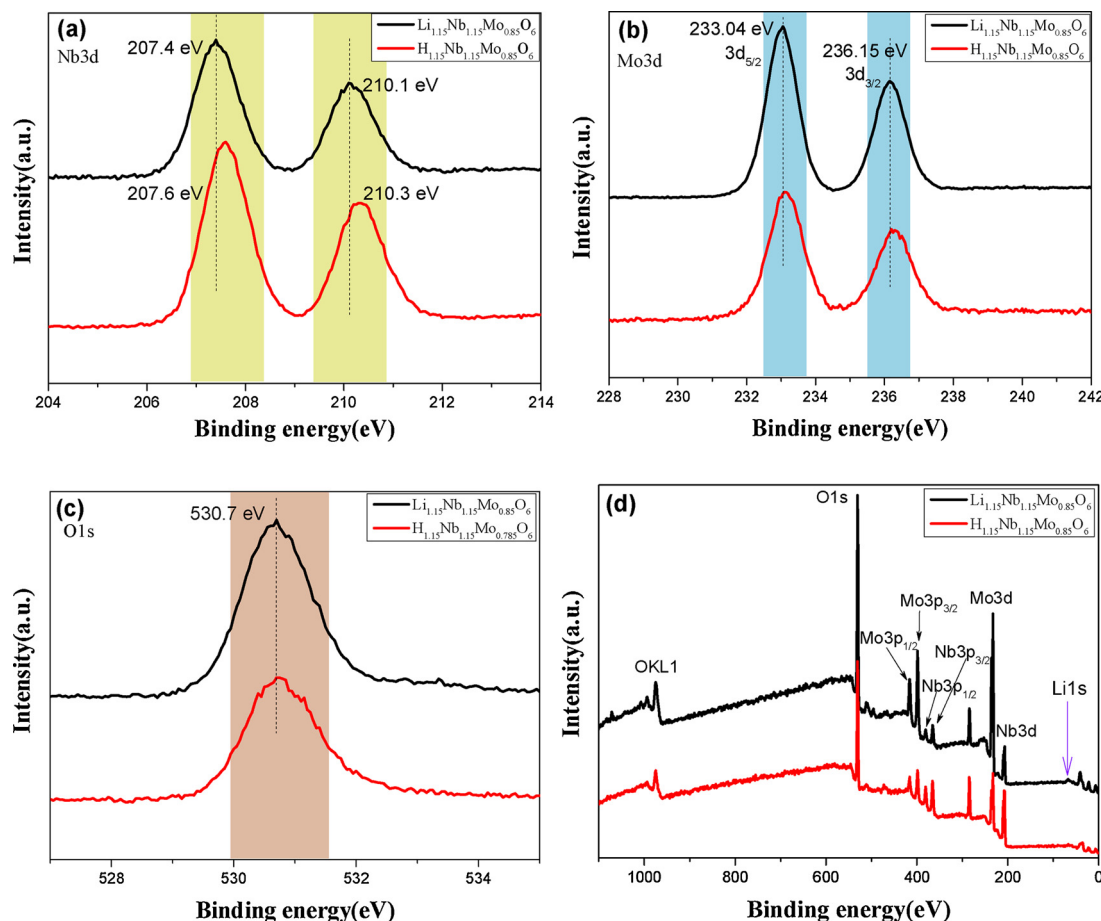


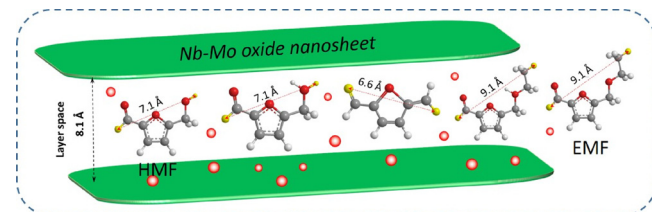
**Fig. 5.** High-resolution XPS spectra of Nb3d, Mo3d and O1s core levels and survey spectra of the  $\text{H}_{1.15}\text{Nb}_{1.15}\text{Mo}_{0.7}\text{O}_6$  and  $\text{Li}_{1.15}\text{Nb}_{1.15}\text{Mo}_{0.85}\text{O}_6$ .

**Table 2**  
Catalytic results of etherification based on different comparative catalysts.

Entries	Catalysts	HMF conversion(%)	EMF Selectivity (%)
1	$\text{LiNbWO}_6$	16.5	trace
2	$\text{LiTaMoO}_6$	12.4	trace
3	$\text{LiNbMoO}_6$	16.2	trace
4	$\text{HNbWO}_6$	17.9	2
5	$\text{HTaMoO}_6$	22.6	11.7
6	$\text{HNbMoO}_6$	93	97

Reaction condition: 1 mmol HMF, 5 ml ethanol, 0.05 g catalyst, 3 h, and 100 °C.

activity even without observable selectivity toward EMF, which is ascribed to lack of the proton acid before introducing the H proton in the interlayer of Nb-Mo oxides. Accordingly, the certain selectivity of EMF was observed in the presence of H proton in the niobium molybdates. This present phenomenon indicates the Brønsted acid site should be the



**Scheme 2.** Description for the existing state of involved reactant molecule and their intermediate in the inlayer space of Nb-Mo oxide nanosheets.

real active center in light of the proceeding catalytic etherification process of HMF rather than Louis acid sites on the Nb or Mo atoms despite the observable catalytic conversion of HMF in the presence of various lithium salts. However, the difference between several polyoxometalates composites acid for the catalytic etherification is

**Table 3**  
Catalytic results based on niobium molybdates catalyst with the tuned proportion of Nb and Mo.<sup>a</sup>

Entries	Catalysts	Nb/Mo <sup>b</sup>	Acid amounts <sup>c</sup> [mmol/g]	HMF conversion(%)	EMF selectivity <sup>d</sup> (%)
1	$\text{H}_{0.7}\text{Nb}_{0.7}\text{Mo}_{1.3}\text{O}_6$	0.697/1.306	1.13	81.2	81
2	$\text{H}_{0.85}\text{Nb}_{0.85}\text{Mo}_{1.15}\text{O}_6$	0.856/1.152	1.32	88.4	93
4	$\text{HNbMoO}_6$	0.985/1.031	1.81	93	97
5	$\text{H}_{1.15}\text{Nb}_{1.15}\text{Mo}_{0.85}\text{O}_6$	1.148/0.847	1.95	100	> 99
6	$\text{H}_{1.3}\text{Nb}_{1.3}\text{Mo}_{0.7}\text{O}_6$	1.302/0.711	1.71	96	96

<sup>a</sup> Reaction condition: 1 mmol HMF, 5 ml ethanol, 0.05 g catalyst, 3 h, and 100 °C.

<sup>b</sup> The results were determined from ICP measurement.

<sup>c</sup> Acid amount was determined by acid titration.

<sup>d</sup> The remaining products excluding EMF are ethyl-4-oxopentanoate (EOP).

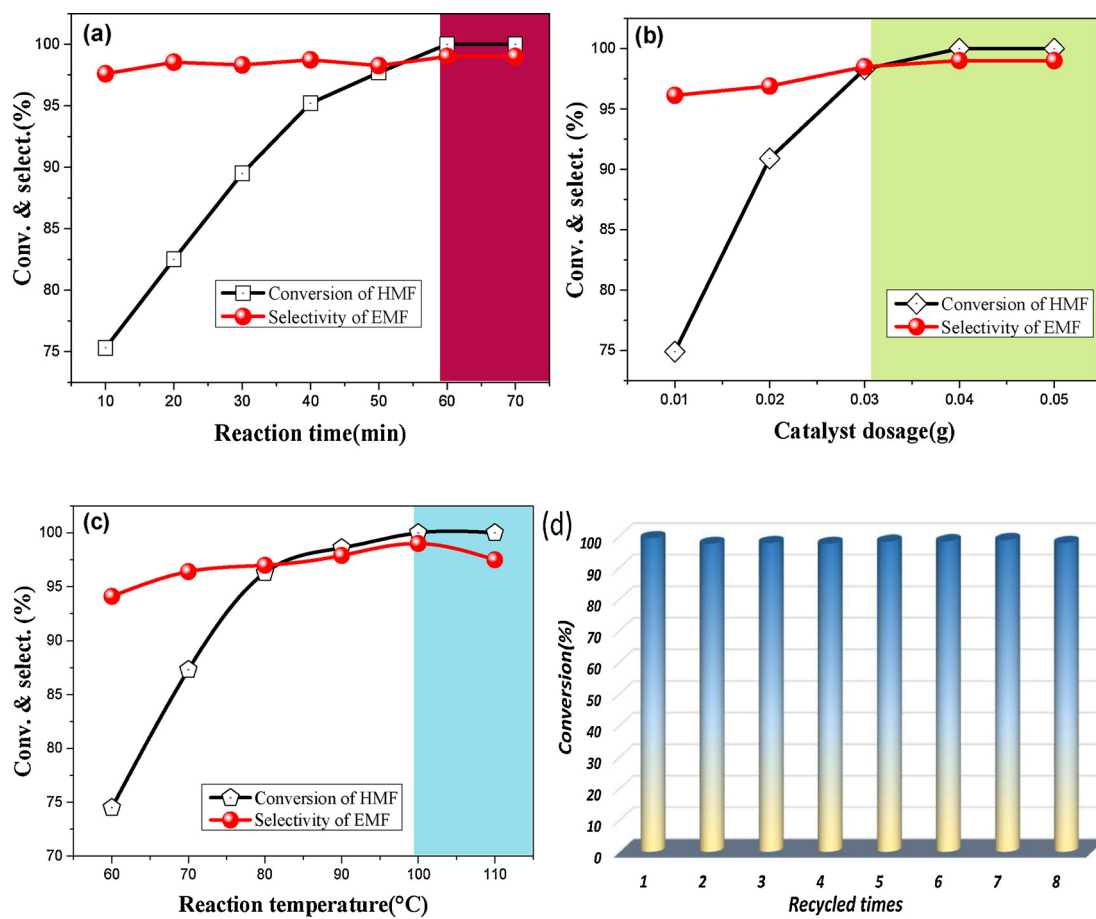


**Fig. 6.** Effects of reaction time on the reaction (a), 1 mmol HMF, 5 ml ethanol, 0.05 g catalyst, and 100 °C; Effects of catalyst dosage on the reaction (b), 1 mmol HMF, 5 ml ethanol, 100 °C, and 1 h. Effects of reaction temperature on the reaction (c), 1 mmol HMF, 5 ml ethanol, 0.05 g catalyst, and 1 h; Stability assessment of the  $\text{H}_{1.15}\text{Nb}_{1.15}\text{Mo}_{0.85}\text{O}_6$  (d).

**Table 4**

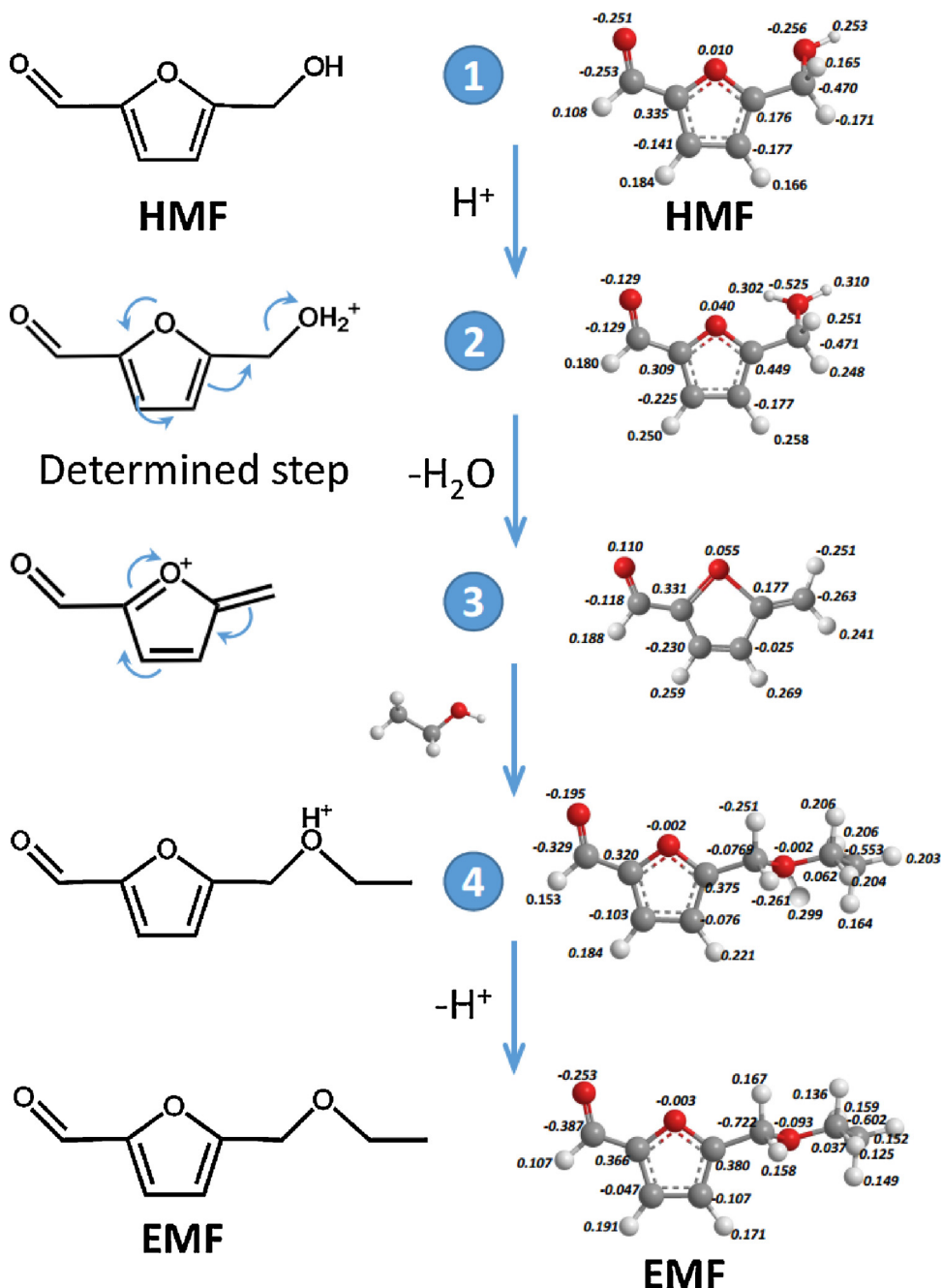
Comparison of the etherification of HMF to EMF with reported different catalysts.

Entry	Catalyst	T/°C	t/h	conv. %	EMF Yield %	ref.
1	H5IW/M-Ns	90	4	92	77.4	[27]
2	$\text{Fe}_3\text{O}_4@\text{SiO}_2$ -HPW	100	11	97.9	83.6	[28]
3	MCM-41-HPW	100	12	96.1	83.4	[29]
4	$\text{Ag}_1\text{H}_2\text{PW}$	100	10	94.4	88.7	[30]
5	$[\text{MIMBSI}]_3\text{PW}_{12}\text{O}_{40}$	70	24	98.1	90.7	[44]
6	$\text{Fe}_3\text{O}_4@\text{SiO}_2\text{-SH-Im-HSO}_4$	100	12	97.9	89.6	[31]
7	$\text{Fe}_3\text{O}_4@\text{C-SO}_3\text{H}$	100	12	94.5	88.4	[45]
8	$\text{Fe}_3\text{O}_4@\text{SiO}_2\text{-SO}_3\text{H}$	100	10	100	89.3	[46]
9	Silica-SO <sub>3</sub> H	100	10	96.5	83.8	[32]
10	SO <sub>3</sub> H-SBA-15-D	140	24	> 99	3.5	[33]
11	H <sub>2</sub> SO <sub>4</sub>	75	24	–	81	[34]
12	p-TSA	75	24	–	75	[34]
13	AlCl <sub>3</sub>	100	5	95	92.9	[47]
14	GO	100	12	96	92	[48]
15	Co(II)Pc&[EMIm]Cl	90	2	–	92	[49]
16	FeCl <sub>3</sub>	100	12	94.2	89.4	[50]
17	CST-1	110	4	99	84	[51]
18	Zr-SBA-15	140	5	100	76	[24]
19	$\text{H}_{1.15}\text{Nb}_{1.15}\text{Mo}_{0.85}\text{O}_6$	100	12	100	> 99	this work

remarkable because of different metal composition in the crystal structure. According to the reported literature [40], HNbMoO<sub>6</sub> afford the relatively stronger acid strength among some polyoxometalates such as HNbMoO<sub>6</sub>, HNbWO<sub>6</sub>, HTiNbO<sub>5</sub> and etc. Based on the analysis of the catalytic capacity of HNbWO<sub>6</sub>, HTaMoO<sub>6</sub>, and HNbMoO<sub>6</sub>, it seems to conclude that the existence and enhancement of Nb are beneficial to

the production of EMF.

Through adjusting the proportion of Nb and Mo in the compound of niobium molybdates, the acid amount is capable of being regulated to some extent, especially when increasing the part of Nb in the entire compound of niobium molybdates, which is in accordance with acid titration results (Table 3), however, the crystalline structure of niobium molybdates is easily damaged to some extent owing to the excessive introduction of Nb or Mo in the original structure of HNbMoO<sub>6</sub>. For instance, the validate acid amount of  $\text{H}_{1.3}\text{Nb}_{1.3}\text{Mo}_{0.7}\text{O}_6$  derived from the titration result presents the lower value which indicates the possible existed structure damage of niobium molybdates and newly-emerged phase of  $\text{Nb}_2\text{O}_5$  or  $\text{Mo}_2\text{O}_3$ , thereby influencing the regular presence of accessible H<sup>+</sup> sites. Meanwhile, the enlargement of interlayer space can be observed with the Nb content, indicating the one-stone-two-birds effect of increasing Nb content. Herein, catalytic etherification capacity using  $\text{H}_{0.7}\text{Nb}_{0.7}\text{Mo}_{1.3}\text{O}_6$ ,  $\text{H}_{0.85}\text{Nb}_{0.85}\text{Mo}_{1.15}\text{O}_6$ , HNbMoO<sub>6</sub>,  $\text{H}_{1.15}\text{Nb}_{1.15}\text{Mo}_{0.85}\text{O}_6$ , and  $\text{H}_{1.3}\text{Nb}_{1.3}\text{Mo}_{0.7}\text{O}_6$  were ulteriorly investigated and their catalytic results are shown in Table 3. As expected, the catalytic activity in conversion was greatly improved based on the increment of the acid amount in light of the  $\text{H}_{1.15}\text{Nb}_{1.15}\text{Mo}_{0.85}\text{O}_6$ . However, the catalytic activity of  $\text{H}_{1.3}\text{Nb}_{1.3}\text{Mo}_{0.7}\text{O}_6$  presents the dropped trend compared to that of aforementioned one because of the damage of structure and existence of performance-poor impure  $\text{Nb}_2\text{O}_5$  or  $\text{Mo}_2\text{O}_3$  after excessively adjusting the proportions of Nb/Mo, which is closely reflected by aforementioned acid amount analysis. In addition, it is observed that the selectivity of EMF was controlled with the adjusted proportion of Nb/Mo, indicating the positive correlation between the catalytic selectivity of EMF and concentration of Nb = O moieties. On the other hand, as evidence, in light of the enhancement of



Scheme 3. The proposed mechanism for etherification steps of HMF with ethanol.

EMF selectivity, the structure-shaped interlayer space adaptability was regarded as the key factor for enhancing the selectivity of EMF, due to the easier production of bigger EMF molecule in the enlarged interlayer space through increasing the element Nb proportion (Scheme 2). In addition, the broader reaction channel is beneficial to stabilize the formed EMF molecule, thereby avoiding its further transformation into chain of EOP. As such, Paola Lanzafame et al. have also demonstrated the great relationship between selectivity of EMF and microstructure of catalyst [42]. Hence, it is inclined to conclude that, on the basis of the present inherent acid active sites, the regulation of reaction channel gives rise to the great adjustable effect on the selectivity of EMF, thereby contributing the high yield of targeted EMF molecule. However, note that the excessive expanding of reaction space is still adverse for the entire reaction owing to the damage of structure and impure Nb or Mo oxides. Therefore, the  $\text{H}_{1.3}\text{Nb}_{1.3}\text{Mo}_{0.7}\text{O}_6$  gives rise to the worse

catalytic activity compared to  $\text{H}_{1.15}\text{Nb}_{1.15}\text{Mo}_{0.85}\text{O}_6$  in light of numbers of active centers. Taken together, the increment of the acid amount and rational enlargement of interlayer space mainly contributed to the nearly full conversion of HMF to EMF via their synergistic effect. In addition, in the second point, we speculated the suppression of side reaction that transformation of EMF to EOP derived from the function of Lewis acid site corresponding to the Nb or Mo species to some extent, which could coordinate the oxygen atom of aldehyde group and stabilize the resultant EMF, thereby avoiding the attack of EtOH and ensuing ring opening of furan owing to the attack of proton acid. This similar influence derived from the Lewis acid site on the EMF was also discerned and verified in the reported literature [42]. To confirm the function of Lewis acid, we tentatively used the  $\text{H}_2\text{SO}_4$  solution containing commercial  $\text{MoO}_3$  and  $\text{Nb}_2\text{O}_5$  particle catalyze the HMF etherification, showing 89% yield of EMF, which affords certain

**Table 5**  
Expanded catalytic etherification experiments using different alcohols.

Entry	Alcohols	Ethers	Time (h)	Yield (%)
1	H <sub>3</sub> C-OH		12	> 99
2	CH <sub>2</sub> -OH		12	> 99
3	CH <sub>2</sub> CH <sub>2</sub> OH		12	93
4	CH <sub>2</sub> CH(OH)CH <sub>3</sub>		12	87
5	CH <sub>2</sub> CH(OH)CH <sub>2</sub> CH <sub>3</sub>		12	75
6	CH <sub>2</sub> CH <sub>2</sub> CH(OH)CH <sub>3</sub>		12	71
7	Phenol		12	53
8	Cyclohexylmethanol		12	57

Reaction conditions: 1 mmol HMF, 5 ml corresponding alcohols, 0.05 g catalyst, 12 h, and 100 °C. Methanol, ethanol, propyl alcohol, isopropanol, *tert*-Butanol, isoamyl alcohol, benzyl alcohol, and cyclohexylmethanol.

enhancement of EMF yield compared to only H<sub>2</sub>SO<sub>4</sub> solution with 80% yield of EMF, implying the above proposed applicable explanation to some extent. However, on the other hand, as a contrast, the sample H<sub>0.7</sub>Nb<sub>0.7</sub>Mo<sub>1.3</sub>O<sub>6</sub> synthesized in this study didn't exhibit the complete generation of EMF and 100% selectivity even affording Brønsted and Lewis acid sites, which should associate with the narrow reaction channel of H<sub>0.7</sub>Nb<sub>0.7</sub>Mo<sub>1.3</sub>O<sub>6</sub> compared with the interlayer-space enlarged H<sub>1.15</sub>Nb<sub>1.15</sub>Mo<sub>0.85</sub>O<sub>6</sub>, thereby giving rise to position steric hindrance for not affording free coordination of bigger EMF with the Lewis acid site for stabilizing aldehyde group in the interlayer space, implying the nonuniqueness of reactivity regulation via only Lewis acid site in this study. Taken together, the high yield of EMF should be attributed to the coupling effect from the regulated reaction interlayer space and stabilized effect of Lewis acid on the EMF.

To explore the optimal reaction condition, the reaction time and the dosage of catalyst, together with reaction temperature were ulteriorly examined and their corresponding results are displayed in Fig. 6a, b, c. As shown, judging from the time course of HMF conversion using H<sub>1.15</sub>Nb<sub>1.15</sub>Mo<sub>0.85</sub>O<sub>6</sub>, the catalytic etherification process affords the ultrafast reaction rate in the only 10 min, whose catalytic conversion reaches nearly 75%. While in the last period of reaction ranging from 10 min to 70 min, the reaction rate shows the slowly-increased trend and the reaction equilibrium was reached at 60 min, indicating the optimal reaction time is 60 min. The effect of catalyst dosage on the catalytic reaction indicates that 0.04 g dosage of catalyst seems enough for providing the acidic sites to catalyze the complete conversion of HMF. The effect of reaction temperature reveals the catalytic conversion can be obviously enhanced from 75% to 100% with the increased reaction temperature from 60 °C to 100 °C, but, note that the catalytic selectivity of EMF gives the first rise and then fall trend with the temperature ranging from 60 °C to 110 °C, especially the drop of selectivity after 100 °C should be attributed to the consumption of EMF to degradation, which verifies the used temperature of 100 °C seems to be optimal reaction temperature. Besides, the real isolated yield was

measured based on the direct rotary evaporation and calculated as 97% which is slightly lower than calculated GC yield. Besides, the NMR spectra(H NMR and C NMR) of the isolated EMF products directly derived from the isolated experiment were displayed in Fig. 5S, demonstrating its purity. This could absolutely confirm the realized high yield by virtue of the present reaction system. Reusability of heterogeneous catalysts is also an important characteristic to evaluate the durable catalytic performance of the prepared catalyst [43]. Therefore, the reusability and stability were further checked based on five recycling of catalytic experiments(Fig. 6d). Impressively, the durable catalytic activity (99% yield) was received during the eight recycling, and no loss of catalytic activity was observed, which further confirms its superiority that stability in the solid acid catalyst for potential industrial application.

To highlight the superiority of the niobium molybdates catalyst, Table 4 and Fig. 6S lists catalytic results involved etherification of HMF over various reported acid catalysts, taking a general survey of catalytic results, the present niobium molybdates catalyst absolutely affords the highest catalytic activity whatever catalytic conversion or selectivity towards EMF in all cases, and emerged as the record-high yield known in these reported solid acid catalyst. Even if some catalysts show the high conversion, the present selectivity of EMF seems undesirable in light of industrial production. This result should be associated with the fact that the present interlayer confinement space exerts the special effect on the catalytic selectivity toward EMF. Therefore, the niobium molybdates catalyst exhibits the potential possibility for industrial production.

Based on the calculation of Mulliken charge of atom in the involved reactant and immediate molecules, the reaction pathways can be referred to in Scheme 3. In the proposed catalytic reaction procedure [52], the formation of EMF from HMF acquired typical four transforming steps including (1) attack of H proton, (2) dehydration, (3) attack and insert of ethanol molecule, and (4) desorption of H proton, among which the dehydration was regarded as the rate-determined step controlling the entire reaction. At the beginning of the reaction, the proton H<sup>+</sup> in the interlayer attracts HMF, forming the protonated HMF, (1→2). Ensuingly, the protonated HMF liberates the H<sub>2</sub>O molecule free (2→3) and produces the isomerized immediate transient state, which then interacts with C<sub>2</sub>H<sub>5</sub>OH through addition reaction where an ether-oxygen bond is forming(3→4), after that, proton H<sup>+</sup> can easily leave and generate the final EMF. In addition, the suppression of side reaction from EMF to EOP could be further identified based on the charge character of resultant product EMF. To our knowledge, the aldehyde group with most negative charge of oxygen atoms on the EMF is most active and easily attacked by protonation under acid condition [53]. Ensuingly, the protonated aldehyde group easily occurs the hemiacetal reaction with ethanol, and followed by the ring opening of furan and arrangement of structure into final EOP. Therefore, the stability of aldehyde group on the EMF by virtue of Lewis acid site derived niobium molybdates catalyst using coordination effect, which could escape from the protonation and succedent side reaction.

In addition, to study the applicability of niobium molybdates catalyst for the catalytic esterification of HMF with other types of alcohols, the expanded catalytic reactions were carried out based on the identical catalytic conditions involved in aforementioned catalytic reaction (Table 5), among which the methanol, ethanol, propyl alcohol, isopropanol, *tert*-Butanol, isoamyl alcohol, benzyl alcohol, and cyclohexylmethanol were used as the contrastive substrates. Notably, the high yield can be received when using the simple alcohol, in turn, the decreasing catalytic activity can be observed from entry 3 to entry 8, which associated with the existed steric hindrance and possible inadequate reaction temperature, prohibiting the efficient progress of the reaction in the interlayer space of niobium molybdate.

On basis of the superior catalytic effect HNbMoO<sub>6</sub> catalyst in light of etherification of HMF to synthesize EMF, which pushes the progress of the direct synthesis EMF using the raw material fructose and ensuing

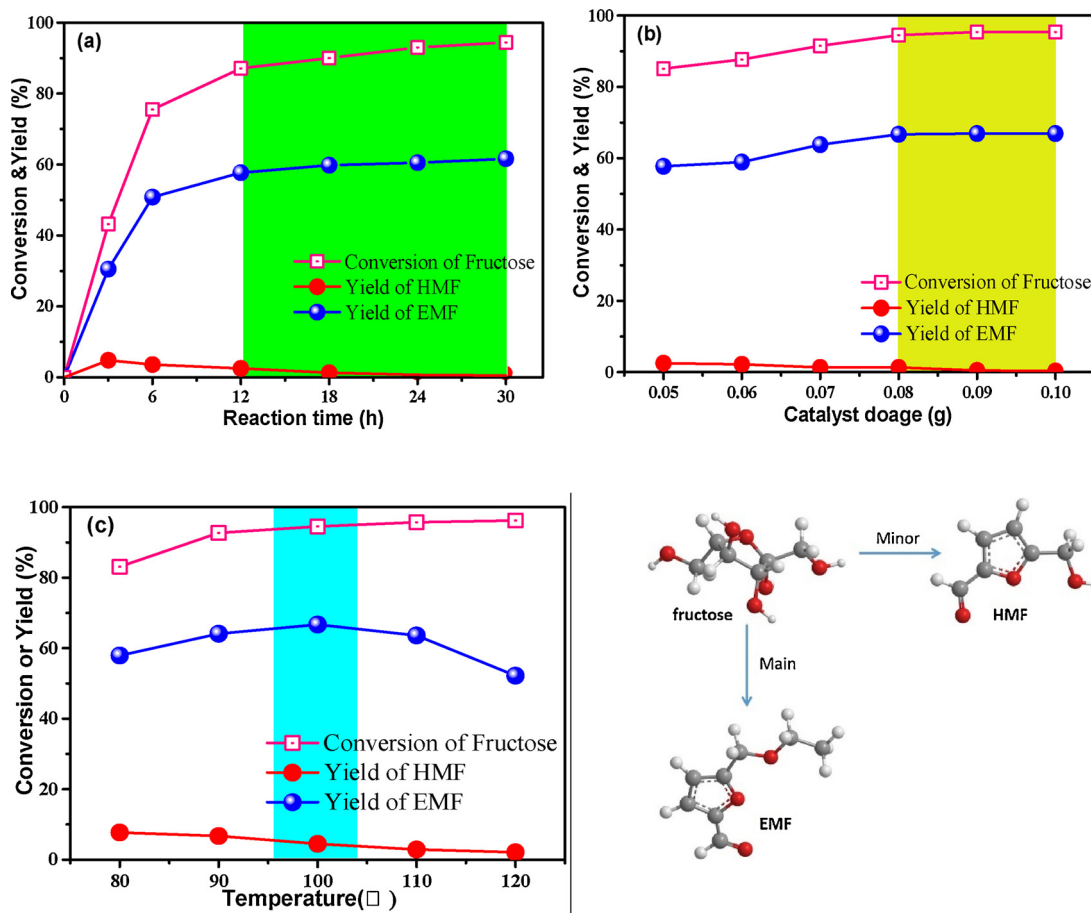


**Fig. 7.** Effect of reaction condition on the direct catalytic conversion of fructose using  $H_{1.15}Nb_{1.15}Mo_{0.85}O_6$ , reaction time (a) 1 mmol fructose, 5 ml ethanol, 0.05 g catalyst, and 100 °C; reaction temperature (b) 1 mmol fructose, 5 ml ethanol, 100 °C, and 12 h; and catalyst dosage (c) 1 mmol fructose, 5 ml ethanol, 0.08 g catalyst, and 12 h.

optimizes the reaction conditions, which might avoid the tedious procedures for the separation of the intermediate HMF. Firstly, the reaction time is checked to obtain the optimal time nodes that 12 h (Fig. 7 a). The conversion rate of fructose has reached about 75%, and the yield of EMF is ca. 52%. Prolonging reaction time, the conversion of fructose and the yield of EMF increased slowly, indicating the almost reaction equilibrium. Ensuingly, the effect of used catalyst dosage on the catalytic result of fructose was investigated, and the yield of EMF changed ranging from 58% to 67% corresponding to the increment of catalyst dosage from 0.05 g to 0.1 g. HMF has been almost completely converted when using 0.08 g of catalyst, and the EMF yield increased to the maximum accordingly, indicating that the  $H_{1.15}Nb_{1.15}Mo_{0.85}O_6$  catalyst can provide enough acid sites to complete dehydration and etherification reaction of fructose. Accordingly, excessive use of the catalyst seems meaningless in light of the reaction based on the reaction proper process [54]. Since the dehydration of fructose to HMF is also the acid-required process and emerged as the competitive reaction, the preparation of EMF from fructose consume more catalyst dosage compared to that using HMF as a raw material.

Finally, reaction temperature-dependent catalytic effect was ulteriorly identified to obtain the optimal reaction temperature for the direct synthesis of EMF from fructose based on the controlled reaction temperature range 80–120 °C, as shown in Fig. 7b, as the continues increment in reaction temperature, and the yield of EMF shows the decreased trend accompanied by the more production of humin. In summary, the optimal reaction temperature is 100 °C. Notably, the yield of HMF from fructose exhibits the decreased trend with prolonged reaction time, increased reaction temperature and catalyst dosage. This is

attributed to the enhanced successive reaction rate of HMF with ethanol in the presence of a more favorable reaction condition. Taken together, the direct synthesis of EMF from the fructose was enabled by niobium molybdates catalyst, but resulted from the limited catalytic capacity of niobium molybdates catalyst in light of catalytic hydrolysis of fructose.

#### 4. Conclusions

In summary, we successfully demonstrated a highly-efficient and stable solid acid catalyst that niobium molybdate with the varied metal components to realize the regulation of acid amount and interlayer space of Nb-Mo oxides layer simultaneously. The adjustable acid properties that acid amounts were received based on the precisely-controlled proportion of metal oxides Nb and Mo in this catalyst. The multiple-layered configuration of the sample was clearly identified based on corresponding characterization techniques. The resulted catalyst show the complete conversion of HMF within short reaction time (60 min), and the value-added EMF was directly and selectively generated by the etherification reaction, which is the highest performance values known among reported solid acid catalysts. Ulteriorly, the direct synthesis of EMF from the fructose was explored using niobium molybdates catalyst, and the high conversion of fructose was demonstrated but accompanied with relatively moderate yield toward EMF(67%) even with the longer reaction time, which resulted from the limited catalytic capacity of niobium molybdates catalyst in light of catalytic hydrolysis of fructose. Extendedly, the niobium molybdates catalyst exhibits the superior catalytic activity towards the etherification of HMF with various alcohols, and exerts high reusable catalytic property

in this etherification process. In light of the excellent catalytic etherification activity and durable catalytic stability, as presented here, might be promising alternatives to replace hazardous and corrosive homogeneous molecular acid catalysts, thus making a significant contribution to green chemistry and industrial production.

## Conflicts of interest

There are no conflicts to declare.

## Acknowledgements

The authors acknowledge the project Funded by the National Natural Science Foundation (51672114), Natural Science Foundation of Jiangsu Province (BK20151328, BK20161357), Foundation from Marine Equipment and Technology Institute for Jiangsu University of Science and Technology (HZ20170015), and Scientific Research Foundation (1112921902) of Jiangsu University of Science & Technology.

## Appendix A. Supplementary data

Supplementary material related to this article can be found, in the online version, at doi:<https://doi.org/10.1016/j.apcatb.2019.117786>.

## References

- [1] X. Chen, Y. Gao, L. Wang, H. Chen, N. Yan, Effect of treatment methods on chitin structure and its transformation into nitrogen-containing chemicals, *Chemppluschem* 80 (2015) 1565–1572.
- [2] X. Chen, H. Yang, N. Yan, Shell biorefinery: dream or reality? *Chem. a Eur. J.* 22 (2016) 13402–13421.
- [3] Y. Gao, X. Chen, J. Zhang, N. Yan, Chitin-derived mesoporous, nitrogen-containing carbon for heavy-metal removal and styrene epoxidation, *ChempPlusChem* 80 (2015) 1556–1564.
- [4] J. Zhang, L. Lombardo, G. Gozaydin, P.J. Dyson, N. Yan, Single-step conversion of lignin monomers to phenol: bridging the gap between lignin and high-value chemicals, *Chin. J. Catal.* 39 (2018) 1445–1452.
- [5] Y. Ren, Z. Yuan, K. Lv, J. Sun, Z. Zhang, Q. Chi, Selective and metal-free oxidation of biomass-derived 5-hydroxymethylfurfural to 2,5-diformylfuran over nitrogen-doped carbon materials, *Green Chem.* 20 (2018) 4946–4956.
- [6] Z. Yuan, B. Liu, P. Zhou, Z. Zhang, Q. Chi, Aerobic oxidation of biomass-derived 5-hydroxymethylfurfural to 2,5-diformylfuran with cesium-doped manganese dioxide, *Catal. Sci. Tech.* 8 (2018) 4430–4439.
- [7] B. Liu, Y. Ren, Z. Zhang, Aerobic oxidation of 5-hydroxymethylfurfural into 2,5-furandicarboxylic acid in water under mild conditions, *Green Chem.* 17 (2015) 1610–1617.
- [8] L. Jiang, H. Guo, C. Li, P. Zhou, Z. Zhang, Selective cleavage of lignin and lignin model compounds without external hydrogen, catalyzed by heterogeneous nickel catalysts, *Chem. Sci.* 10 (2019) 4458–4468.
- [9] F. Yang, J. Tang, Catalytic Upgrading of renewable levulinic acid to levulinic esters using perchloric acid decorated nanoporous silica gels, *ChemistrySelect* 4 (2019) 1403–1409.
- [10] J. Pan, H. Gao, Y. Zhang, J. Zeng, W. Shi, C. Song, Y. Yan, L. Yu, D. Chang, Porous solid acid with high Surface area derived from emulsion templating and hyper-crosslinking for efficient one-pot conversion of cellulose to 5-hydroxymethylfurfural, *RSC Adv.* 4 (2014) 59175–59184.
- [11] T. Chen, L. Peng, X. Yu, L. He, Magnetically recyclable cellulose-derived carbonaceous solid acid catalyzed the biofuel 5-ethoxymethylfurfural synthesis from renewable carbohydrates, *Fuel* 219 (2018) 344–352.
- [12] H. Li, S. Saravanamurugan, S. Yang, A. Riisager, Direct transformation of carbohydrates to the biofuel 5-ethoxymethylfurfural by solid acid catalysts, *Green Chem.* 18 (2016) 726–734.
- [13] B. Liu, Z. Zhang, K. Huang, Cellulose sulfuric acid as a bio-supported and recyclable solid acid catalyst for the synthesis of 5-hydroxymethylfurfural and 5-ethoxymethylfurfural from fructose, *Cellulose* 20 (2013) 2081–2089.
- [14] K. Zhao, S. Liu, K. Li, Z. Hu, Y. Yuan, L. Yan, H. Guo, X. Luo, Fabrication of  $-SO_3H$  functionalized aromatic carbon microspheres directly from waste Camellia oleifera shells and their application on heterogeneous acid catalysis, *Mol. Catal.* 433 (2017) 193–201.
- [15] J. He, M. Liu, K. Huang, T.W. Walker, C.T. Maravelias, J.A. Dumesic, G.W. Huber, Production of levoglucosanone and 5-hydroxymethylfurfural from cellulose in polar aprotic solvent-water mixtures, *Green Chem.* 19 (2017) 3642–3653.
- [16] R. Weingarten, A. Rodriguez-Beuerman, F. Cao, J.S. Luterbacher, D.M. Alonso, J.A. Dumesic, G.W. Huber, Selective conversion of cellulose to hydroxymethylfurfural in polar aprotic solvents, *ChemCatChem* 6 (2014) 2229–2234.
- [17] J. Dai, L. Zhu, D. Tang, X. Fu, J. Tang, X. Guo, C. Hu, Sulfonated polyaniline as a solid organocatalyst for dehydration of fructose into 5-hydroxymethylfurfural, *Green Chem.* 19 (2017) 1932–1939.
- [18] C. Fan, H. Guan, H. Zhang, J. Wang, S. Wang, X. Wang, Conversion of fructose and glucose into 5-hydroxymethylfurfural catalyzed by a solid heteropolyacid salt, *Biomass Bioenergy* 35 (2011) 2659–2665.
- [19] S.J. Oh, J. Park, J.G. Na, Y.K. Oh, Y.K. Chang, Production of 5-hydroxymethylfurfural from agarose by using a solid acid catalyst in dimethyl sulfoxide, *RSC Adv.* 5 (2015) 47983–47989.
- [20] L. Wang, H. Wang, F. Liu, A. Zheng, J. Zhang, Q. Sun, J.P. Lewis, L. Zhu, X. Meng, F.-S. Xiao, Selective catalytic production of 5-hydroxymethylfurfural from glucose by adjusting catalyst wettability, *ChemSusChem* 7 (2014) 402–406.
- [21] Y. Bai, L. Wei, M. Yang, H. Chen, S. Holdren, G. Zhu, D.T. Tran, C. Yao, R. Sun, Y. Pan, D. Liu, Three-step cascade over a single catalyst synthesis of 5-(ethoxymethyl)furfural from glucose over a hierarchical lamellar multi-functional zeolite catalyst, *J. Mater. Chem. A Mater. Energy Sustain.* 6 (2018) 7693–7705.
- [22] C.M. Lew, N. Rajabbeigi, M. Tsapatsis, One-pot synthesis of 5-(ethoxymethyl)furfural from glucose using sn-bea and amberlyst catalysts, *Ind. Eng. Chem. Res.* 51 (2012) 5364–5366.
- [23] P.K. Kumari, B.S. Rao, D. Padmakar, N. Pasha, N. Lingaiah, Lewis acidity induced heteropoly tungstate catalysts for the synthesis of 5-thoxymethyl furfural from fructose and 5-hydroxymethylfurfural, *Mol. Catal.* 448 (2018) 108–115.
- [24] P. Lanzafame, D.M. Temi, S. Perathoner, G. Centi, A. Macario, A. Aloise, G. Giordano, Etherification of 5-hydroxymethyl-2-furfural (HMF) with ethanol to biodiesel components using mesoporous solid acidic catalysts, *Catal. Today* 175 (2011) 435–441.
- [25] L. Hu, G. Zhao, W. Hao, X. Tang, Y. Sun, L. Lin, S. Liu, Catalytic conversion of biomass-derived carbohydrates into fuels and chemicals via furanic aldehydes, *RSC Adv.* 2 (2012) 11184–11206.
- [26] J. Li, Y. Wang, B. Lu, Y. Wang, T. Deng, X. Hou, Protonic acid catalysis of sulfonated carbon material: tunable and selective conversion of fructose in low-boiling point solvent, *Appl. Catal. A-Gen.* 566 (2018) 140–145.
- [27] P. Che, F. Lu, J. Zhang, Y. Huang, X. Nie, J. Gao, J. Xu, Catalytic selective etherification of hydroxyl groups in 5-hydroxymethylfurfural over  $H_4SiW_{12}O_{40}/MCM-41$  nanospheres for liquid fuel production, *Bioresour. Technol.* 119 (2012) 433–436.
- [28] S. Wang, Z. Zhang, B. Liu, J. Li, Silica coated magnetic  $Fe_3O_4$  nanoparticles supported phosphotungstic acid: a novel environmentally friendly catalyst for the synthesis of 5-ethoxymethylfurfural from 5-hydroxymethylfurfural and fructose, *Catal. Sci. Tech.* 3 (2013) 2104–2112.
- [29] A. Liu, Z. Zhang, Z. Fang, B. Liu, K. Huang, Synthesis of 5-ethoxymethylfurfural from 5-hydroxymethylfurfural and fructose in ethanol catalyzed by MCM-41 supported phosphotungstic acid, *J. Ind. Eng. Chem.* 20 (2014) 1977–1984.
- [30] Y. Ren, B. Liu, Z. Zhang, J. Lin, Silver-exchanged heteropolyacid catalyst ( $Ag_2H_2PW$ ): an efficient heterogeneous catalyst for the synthesis of 5-ethoxymethylfurfural from 5-hydroxymethylfurfural and fructose, *J. Ind. Eng. Chem.* 21 (2015) 1127–1131.
- [31] S. Yin, J. Sun, B. Liu, Z. Zhang, Magnetic material grafted cross-linked imidazolium based polyionic liquids: an efficient acid catalyst for the synthesis of promising liquid fuel 5-ethoxymethylfurfural from carbohydrates, *J. Mater. Chem. A Mater. Energy Sustain.* 3 (2015) 4992–4999.
- [32] B. Liu, Z. Zhang, One-pot conversion of carbohydrates into 5-ethoxymethylfurfural and ethyl D-glucopyranoside in ethanol catalyzed by a silica supported sulfonic acid catalyst, *RSC Adv.* 3 (2013) 12313–12319.
- [33] S. Saravanamurugan, A. Riisager, Solid acid catalysed formation of ethyl levulinate and ethyl glucopyranoside from mono- and disaccharides, *Catal. Commun.* 17 (2012) 71–75.
- [34] M. Balakrishnan, E.R. Sacia, A.T. Bell, Etherification and reductive etherification of 5-(hydroxymethyl)furfural: 5-(alkoxymethyl)furfurals and 2,5-bis(alkoxymethyl)furan as potential bio-diesel candidates, *Green Chem.* 14 (2012) 1626–1634.
- [35] C. Tagusagawa, A. Takagaki, S. Hayashi, K. Domen, Efficient utilization of nanospace of layered transition metal oxide  $HnBMoO_6$  as a strong, water-tolerant solid acid catalyst, *J. Am. Chem. Soc.* 130 (2008) 7230–7231.
- [36] C. Tagusagawa, A. Takagaki, K. Takanabe, K. Ebitani, S. Hayashi, K. Domen, Effects of transition-metal composition of protonated, layered nonstoichiometric oxides  $H_1-Nb_{1-x}Mo_{1+x}O_6$  on heterogeneous acid catalysis, *J. Phys. Chem. C* 113 (2009) 17421–17427.
- [37] S. Shetsiri, A. Thivatasith, K. Saenluang, W. Wannapakdee, S. Salakhum, P. Wetchasat, S. Nokbin, J. Limtrakul, C. Wattanakit, Sustainable production of ethylene from bioethanol over hierarchical ZSM-5 nanosheets, *Sustain. Energy Fuels* 3 (2019) 115–126.
- [38] P. Shen, H.T. Zhang, H. Liu, J.Y. Xin, L.F. Fei, X.G. Luo, R.Z. Ma, S.J. Zhang, Core-shell  $Fe_3O_4@SiO_2@HnBMoO_6$  nanocomposites: new magnetically recyclable solid acid for heterogeneous catalysis, *J. Mater. Chem. A Mater. Energy Sustain.* 3 (2015) 3456–3464.
- [39] H. Liu, L. Peng, N. Xue, X. Guo, W. Ding, W. Yang, Z. Xie, The effects of carbonaceous species in HZSM-5 on methanol-to-olefin process, *Appl. Catal. A-Gen.* 421 (2012) 108–113.
- [40] J. He, Q.J. Li, Y. Tang, P. Yang, A. Li, R. Li, H.Z. Li, Characterization of  $HnBMoO_6$ ,  $HnBWO_6$  and  $HTiNbO_5$  as solid acids and their catalytic properties for esterification reaction, *Appl. Catal. A-Gen.* 443 (2012) 145–152.
- [41] C.R. Kumar, P.S.S. Prasad, N. Lingaiah, Aluminium exchanged heteropoly tungstate supported on titania catalysts: the generation of Lewis acidity and its role for benzylation reaction, *J. Mol. Catal. A-Chem.* 350 (2011) 83–90.
- [42] P. Lanzafame, K. Barbera, G. Papanikolaou, S. Perathoner, G. Centi, M. Migliori, E. Catizzone, G. Giordano, Comparison of  $H^+$  and  $NH_4^+$  forms of zeolites as acid catalysts for HMF etherification, *Catal. Today* 304 (2018) 97–102.

- [43] F. Yang, B. Shao, X. Liu, S. Gao, X. Hu, M. Xu, Y. Wang, S. Zhou, Y. Kong, Nanosheet-like Ni-based metasilicate towards the regulated catalytic activity in styrene oxidation via introducing heteroatom metal, *Appl. Surf. Sci.* 471 (2019) 822–834.
- [44] L. Bing, Z. Zhang, K. Deng, Efficient one-pot synthesis of 5-(Ethoxymethyl)furfural from fructose catalyzed by a novel solid catalyst, *Ind. Eng. Chem. Res.* 51 (2012) 15331–15336.
- [45] Z. Yuan, Z. Zhang, J. Zheng, J. Lin, Efficient synthesis of promising liquid fuels 5-ethoxymethylfurfural from carbohydrates, *Fuel* 150 (2015) 236–242.
- [46] Z. Zhang, Y. Wang, Z. Fang, B. Liu, Synthesis of 5-Ethoxymethylfurfural from fructose and inulin catalyzed by a magnetically recoverable acid catalyst, *ChemPlusChem* 79 (2014) 233–240.
- [47] B. Liu, Z. Zhang, K. Huang, Z. Fang, Efficient conversion of carbohydrates into 5-ethoxymethylfurfural in ethanol catalyzed by AlCl<sub>3</sub>, *Fuel* 113 (2013) 625–631.
- [48] H. Wang, T. Deng, Y. Wang, X. Cui, Y. Qi, X. Mu, X. Hou, Y. Zhu, Graphene oxide as a facile acid catalyst for the one-pot conversion of carbohydrates into 5-ethoxymethylfurfural, *Green Chem.* 15 (2013) 2379–2383.
- [49] K.K. Yadav, S. Ahmad, S.M.S. Chauhan, Elucidating the role of cobalt phthalocyanine in the dehydration of carbohydrates in ionic liquids, *J. Mol. Catal. A-Chem.* 394 (2014) 170–176.
- [50] X. Zhou, Z. Zhang, B. Liu, Q. Zhou, S. Wang, K. Deng, Catalytic conversion of fructose into furans using FeCl<sub>3</sub> as catalyst, *J. Ind. Eng. Chem.* 20 (2014) 644–649.
- [51] P.A. Russo, M.M. Antunes, P. Neves, P.V. Wiper, E. Fazio, F. Neri, F. Barreca, L. Mafra, M. Pillinger, N. Pinna, A.A. Valente, Solid acids with SO<sub>3</sub>H groups and tunable surface properties: versatile catalysts for biomass conversion, *J. Mater. Chem. A Mater. Energy Sustain.* 2 (2014) 11813–11824.
- [52] E.R. Sacia, M. Balakrishnan, A.T. Bell, Biomass conversion to diesel via the etherification of furanyl alcohol catalyzed by Amberlyst-15, *J. Catal.* 313 (2014) 70–79.
- [53] J.R. Kean, A.E. Graham, Indium(III) triflate promoted synthesis of alkyl levulinates from furyl alcohols and furyl aldehydes, *Catal. Commun.* 59 (2015) 175–179.
- [54] F. Yang, J. Tang, B. Shao, S. Gao, X. Liu, Ni-bearing nanoporous alumina loaded ultralow-concentrated Pd as robust dual catalyst toward hydrogenation and oxidation reactions, *Nano-structures Nano-objects* 18 (2019) 100287–100300.